Organic Electronics 22 (2015) 154–159

Contents lists available at ScienceDirect

Organic Electronics

journal homepage: www.elsevier.com/locate/orgel

Effect of coupling between excitons and gold nanoparticle surface plasmons on emission behavior of phosphorescent organic light-emitting diodes

Wenyu Ji [a,b], Haifeng Zhao [a], Haigui Yang [a,*], Furong Zhu [b,*]

[a] State Key Laboratory of Luminescence and Applications, Changchun Institute of Optics, Fine Mechanics and Physics, Chinese Academy of Sciences, Changchun 130033, China
[b] Department of Physics, Institute of Advanced Materials, and Institute of Research and Continuing Education (Shenzhen), Hong Kong Baptist University, 224 Waterloo Road, Kowloon Tong, NT, Hong Kong

ARTICLE INFO

Article history:
Received 19 September 2014
Received in revised form 17 January 2015
Accepted 31 March 2015
Available online 1 April 2015

Keywords:
Phosphorescent organic light-emitting diodes
Gold nanoparticle
Surface plasmons

ABSTRACT

Enhanced efficiency and reduced efficiency roll-off in phosphorescent organic light-emitting diodes (PhOLEDs) are realized by interposing a solution-processed gold nanoparticle (GNP)-based interlayer between the anode and the hole-injection layer. Transient photoluminescence measurements elucidate that a reduced lifetime of the triplet excitons was observed for samples having a GNP-interlayer as compared to a control sample without the GNP-interlayer. The decrease in the triplet exciton lifetime, caused by the coupling between the triplet excitons and the localized surface plasmons (LSPs) excited by the GNPs, enables reducing the triplet–triplet and triplet–polaron annihilation processes, thereby a reduced efficiency roll-off in PhOLEDs. The presence of a GNP-interlayer also acts as an optical out-coupling layer contributing to the efficiency enhancement and was demonstrated by the theoretical simulation.

1. Introduction

Phosphorescent organic light-emitting diodes (PhOLEDs) have attracted a significant attention for application in flat panel displays and solid-state lighting [1,2]. Many progresses have been made in improving the performance of PhOLEDs, including high power efficiency tandem structure incorporating bulk heterojunction organic bipolar charge generation layer [3]. The accomplishment in bi-directional and symmetrical illumination semitransparent white PhOLEDs also offer additional features and design freedoms for application in planar diffused lighting [4]. Phosphorescent iridium complex based emitters, e.g., fac-tris(2-phenylpyridinato-N,C2′)iridium(III) [Ir(ppy)$_3$] doped in 4,4′-bis(9-carbazolyl)-1,1′-biphenyl (CBP) host, have been widely used. The phosphorescent emitters allow harvesting both singlet and triplet excitons achieving 100% internal quantum efficiency [5], opening up a plethora of opportunities for making highly efficient PhOLEDs. However, there is still a room for further improvement in the efficiency via device optimization. Efficiency roll-off in PhOLEDs, a decrease in the electroluminescence (EL) efficiency at a high current density or luminance, still remains an open challenge. Efficiency roll-off in PhOLEDs is predominantly caused by the triplet–triplet annihilation (TTA) and the triplet–polaron annihilation (TPA) due to the long radiative lifetime of the triplet excitons [6,7]. Different methods have been proposed to reduce the efficiency roll-off in PhOLEDs [8–13]. It is well known that the exciton quenching process due to TTA is proportional to the square of the density of triplet excitons, while the exciton quenching arising from TPA increases linearly with the density of the triplet excitons [9]. Under operation condition, the exciton density is in proportion to the exciton lifetime [7]. Consequently, the TTA is proportional to the square of lifetime of triplet exciton and the TPA scales linearly with the lifetime of triplet exciton. Zhang et al. reported using a short-lived organoeuropium emitter to reduce efficiency roll-off [14], revealing the impact of decrease in the lifetime of triplet excitons on reduced efficiency roll-off in PhOLEDs.

Noble metal nanoparticles have generated considerable interest in recent years due to their unique optical properties that are clearly different from those of the bulk [15–19]. One of these properties is localized surface plasmon (LSP) resonance, which strongly affects the kinetic characteristics of nearby molecules [20]. The incorporation of gold nanoparticles (GNPs) in organic light-emitting diodes (OLEDs) has shown to enhance device performance, due to the LSP effect [21–24]. The effect of GNPs on light out-coupling efficiency in OLEDs is less reported. A systematic study is a prerequisite for better understanding the effect of GNPs on the overall performance of PhOLEDs.

* Corresponding authors.
E-mail addresses: yanghg@ciomp.ac.cn (H. Yang), frzhu@hkbu.edu.hk (F. Zhu).

http://dx.doi.org/10.1016/j.orgel.2015.03.053
1566-1199/

In this work, the performance of GNP-incorporated PhOLEDs, with a distribution of GNPs over the diameter range from 9 to 15 nm on ITO/glass substrates, was investigated. Time-resolved photoluminescence (PL) measurements were used to study the change in the decay rate of triplet excitons in $Ir(ppy)_3$ doped in CBP host, an archetypical electrophosphorescent material system, due to the interaction between triplet excitons and GNPs. Out-coupling effect of GNP-interlayer in PhOLEDs was measured and analyzed using theoretical simulation.

2. Experiments

A set of PhOLEDs, with a structure of glass/ITO/GNPs/MoO_3 (2.0 nm)/CBP (13 nm)/CBP:$Ir(ppy)_3$ (12 wt%, 30 nm)/1,3,5-tri (1-phenyl-1H-benzo[d]imidazol-2-yl)phenyl (TPBi, 45 nm)/LiF (1.0 nm)/Al (100 nm), was fabricated. In this device configuration, MoO_3, CBP, CBP:$Ir(ppy)_3$, TPBi, and LiF/Al were used as the hole injection layer (HIL), hole transporting layer (HTL), green emission layer, electron transporting layer (ETL), and cathode, respectively. Following a previous work [24], a stack of a 2.0 nm thick MoO_3 HIL and a 13 nm thick CBP HTL was adopted, serving as a spacer to optimize the emission output of PhOLEDs. The layer thickness and deposition rate of the materials were monitored *in situ* using an oscillating quartz thickness monitor and the deposition rate of the functional organic materials, LiF and metal cathode was controlled at 0.2, 0.01, and ~0.5 nm/s, respectively. GNP-covered ITO/glass substrates with different GNP concentrations were formed by spin-coating GNP-solutions on the substrates following an annealing at 350 °C in air. Optical density (or absorbance) measurements were carried for solutions with different GNP concentrations. Optical density (OD) is a logarithmic ratio of light falling upon GNP solution to light transmitted through the solution. In this work, PhOLEDs made with GNP-covered ITO/glass substrates, using GNP solutions with different OD values estimated at light wavelength of 540 nm, e.g., devices A (OD = 26), B (OD = 20), and C (OD = 13), were fabricated. The GNPs were chemically synthesized according to the previous literature [25] and the values of the OD were estimated from the diluted GNP solution. A control device having an identical structure made with a bare ITO anode, device D, was also fabricated for comparison studies. The current density–voltage–luminance characteristics and EL spectra of the PhOLEDs were measured by a programmable Keithley model 2400 power supply and a Photo-research PR650 spectrometer at room temperature in air. The devices were not encapsulated. A set of samples having a stack of MoO_3 (2.0 nm)/CBP (13 nm)/CBP:$Ir(ppy)_3$ (30 nm) functional layers on GNP-coated ITO substrates, formed using GNP solutions having different OD values of 26 (S1), 20 (S2), 13 (S3), and a control stack without the GNP-based interlayer (S4) for comparison studies, were prepared. The absorption spectra were measured by an ultraviolet/visible spectrometer (UV 1700, Shimadzu). Transient PL measurements were carried out using Edinburgh Instruments FL920 Spectrometer, using a pulsed laser (average power of ~5 mW) with the wavelength of 405 nm and pulse duration of ~79 ps. All the GNP interlayers on substrates, formed with GNPs in toluene with different OD values, were spin-coated at 1600 rpm and annealed at 350 °C in a glove box (MBRAUN) for 30 min. The morphology of the GNP-covered ITO surfaces with different GNP densities was analyzed using Scanning Electron Microscope (SEM) (Hitachi S4800).

3. Results and discussion

SEM images measured for GNP-covered ITO/glass surfaces having different GNP concentrations, deposited using GNP solutions with different OD values of (a) 26, (b) 20 and (c) 13, are shown in Fig. 1. GNPs on ITO surface have a GNP distribution over the diameter range from 9 to 15 nm. It is clear that GNP-covered ITO with high GNP density generally form relatively larger-sized GNPs, induced by the aggregation of GNPs and the post-annealing process. The coverage of GNPs on ITO surface decreases with the reduction in the concentration of GNPs in the solution. Fig. 2a shows the normalized absorption spectra measured for samples

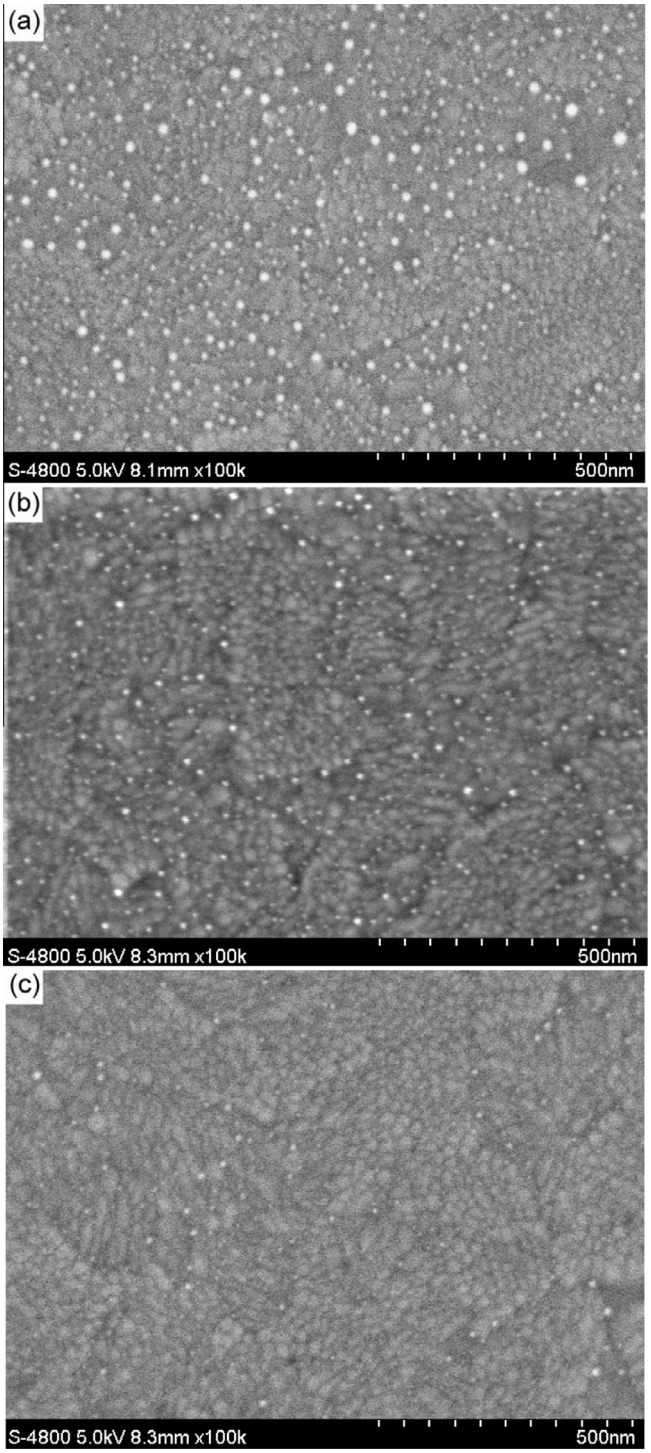

Fig. 1. SEM images measured for GNP-covered ITO/glass surfaces having different GNP concentrations, made by GNP solutions with different OD values of (a) 26, (b) 20 and (c) 13.

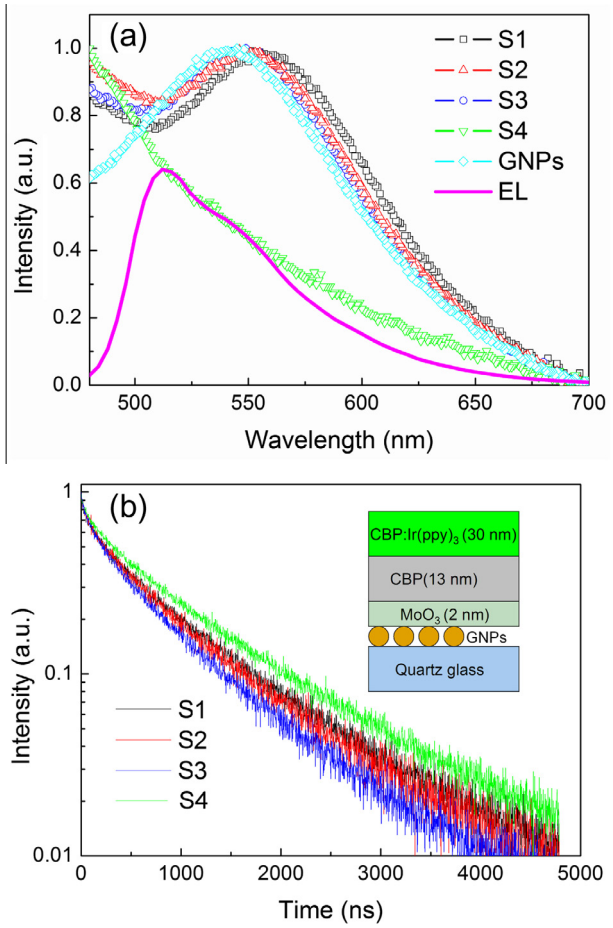

Fig. 2. (a) Absorption spectra measured for four samples having a stack of MoO_3 (2.0 nm)/CBP (13 nm)/CBP:Ir(ppy)$_3$ (30 nm) functional layers on GNP-coated quartz substrates, formed using GNP solutions having different OD values of 26 (S1), 20 (S2), 13 (S3), and a control stack without the GNP-based interlayer (S4) for comparison studies. (b) The corresponding characteristics of transient PL decay from samples S1, S2, S3 and S4. Inset in (b): the cross sectional view of samples having different GNP-interlayers sandwiched between the quartz and the stack of functional layers for time-resolved PL measurements.

S1, S2, S3, S4, and the control specimen with a thin layer of GNPs on ITO glass, formed using the same fabrication condition as that for sample S1. The absorption spectrum measured for the pure GNPs shows a LSP peak at 540 nm. A red-shift in the LSP resonant peak measured for other samples (S1, S2, and S3) is clearly observed as compared to that of the control specimen (S4) as shown in Fig. 2a. The energy of plasmon excitations of GNPs is closely related to the surrounding medium. The GNPs in samples S1, S2 and S3 are covered with a stack of MoO_3 (2.0 nm)/CBP (13 nm)/CBP:Ir(ppy)$_3$ (30 nm) functional layers, different from those in the control specimen that are surrounded by air. Change in the surrounding environment around GNPs could affect the plasmon oscillation frequency, due to the varying ability accommodating the change in the density and the distribution of electrons on the surface of the GNPs [26]. It shows that the LSP resonant peak observed for samples S1, S2 and S3 red shifts with increase in the density of GNPs in the interlayer, shown in Fig. 2a. The red shift of the LSP resonant peak is due to (1) the change in the topography of GNPs during the post annealing process, e.g., agglomeration of GNPs takes place at high GNP density, and (2) a stronger interaction which occurs as the distance between the adjacent GNPs gets closer. The EL spectrum measured for a control PhOLED without the GNP-based interlayer, e.g., glass/ITO/MoO_3 (2.0 nm)/CBP (13 nm)/CBP:Ir(ppy)$_3$ (12 wt%, 30 nm)/TPBi (45 nm)/LiF (1.0 nm)/Al (100 nm), is also shown in Fig. 2a. It can be seen that the absorption spectrum of the GNPs overlaps well with the EL spectrum of the control PhOLED, which is a prerequisite for realizing resonant coupling between the LSP modes and excitons in the PhOLEDs.

In order to examine the effect of GNP-covered ITO anode on the PL decay of the emissive layer, samples with a structurally identical organic stack but without the Al contact was employed for the PL decay measurements. This enables avoiding the influence of Al cathode on PL decay, so as to ascertain the effect of GNPs on the exciton decay processes. Fig. 2b shows the change in the PL decay rate in samples S1, S2, S3 and S4. The cross sectional view of the samples is shown in the inset of Fig. 2b. A bilayer MoO_3 (2.0 nm)/CBP (13 nm) spacer is sandwiched between the phosphorescent layers and GNP-based interlayer. The time-resolved PL measurements were conducted using a pulsed excitation laser with the wavelength of 405 nm, which is below the absorption edge of CBP film [24], while the signals were collected at a wavelength of 512 nm in the PL decay measurements. The difference in the PL decay rate observed for the samples having different GNP concentrations implies that the density of GNP impacts the lifetime of the triplet excitons. For GNP-interlayer having a low GNP density, the LSPs excited by the GNPs can only influence a small amount of the excitons in the emission layer. Hence the reduction in the lifetime of the triplet excitons is less tangible. However, a substantial increase in the PL decay rate was seen when the concentration of GNPs in the interlayer increases, caused by the stronger interaction between the excitons and LSPs, leading toward an obvious decrease in the lifetime of the triplet excitons. As can be seen from Fig. 2b, a faster PL decay rate is observed in samples with higher density of GNPs, reflecting an impact of GNPs on reducing the lifetime of the triplet excitons in CBP:Ir(ppy)$_3$. In order to eliminate the influence of MoO_3 and ITO on the lifetime of excitons, a reference sample (S5), e.g., a stack of CBP (13 nm)/CBP:Ir(ppy)$_3$ (30 nm) on a quartz substrate was also fabricated for time-resolved PL measurement. The results of the PL decay rate measurements show that S4 and S5 possess the same exciton lifetime. The PL decay indicates that the lifetime of the triplet excitons of ~1.0 μs measured for sample S4 is equal to the known lifetime of the triplet excitons in Ir(ppy)$_3$. In contrary, when the interlayers with different GNP densities are incorporated in the samples, e.g., formed using GNP solutions having different OD values of 26 (S1), 20 (S2), 13 (S3), the lifetime of the triplet excitons decreases to 0.72 μs (S1), 0.80 μs (S2), and 0.86 μs (S3), respectively.

The reduction in the lifetime of the triplet excitons in samples S1, S2, and S3 is attributed to the interaction between the excitons in the CPB:Ir(ppy)$_3$ layer and LSPs induced by GNPs. The possible coupling mechanism is illustrated schematically in Fig. 3. The optimum density of GNPs in the samples can be determined according to the assumptions reported by Jung et al. [27] that effective surface plasmons occur within a vicinity of the surface of GNPs from 10 to 70 nm, and the luminescence intensity increases due to coupling between the excitons and LSPs of GNPs. As a consequence, the excitons in the emissive layer can recombine via either radiative or non-radiative decay through the interaction between the excitons and the LSPs. An overlap in the electromagnetic field originated from agglomerated GNPs induces a non-radiative decay of the excitons, due to the destructive interference with the LSPs. More specifically, when a GNP-based interlayer exists at a distance from 10 to 70 nm away from the emissive layer, and the emission wavelength of emitter is close to the resonant wavelength of LSPs, the energy transfer between excitons and LSPs occurs. LSPs have a very large density of states and high local electromagnetic field near the surface of GNPs. A high PL decay rate is then expected due to the strong coupling between the exticons and LSPs. It shows

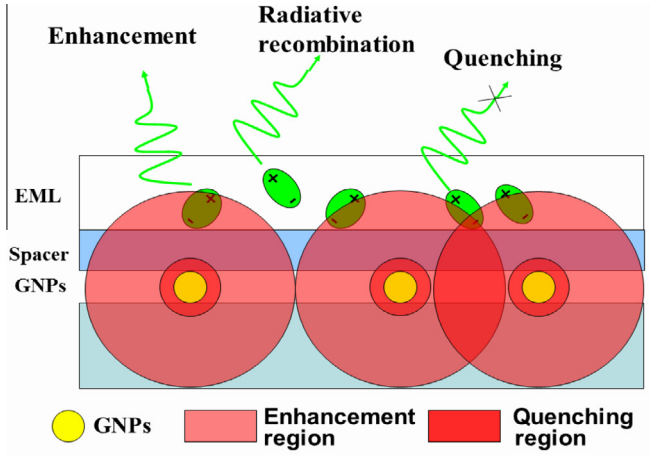

Fig. 3. Schematic diagram illustrating the coupling processes between the excitons and the localized surface plasmons excited by the GNPs.

that not only the distance between the emitter and GNPs, but also the distance between the adjacent GNPs in the interlayer plays an important role in determining the coupling between LSPs and excitons in PhOLEDs. A high density of GNPs in the interlayer will result in an exciton quenching, induced by a strong overlap coupling between the excitons and plasmon excitations of the GNPs.

Fig. 4 shows the luminous efficiency–current efficiency characteristics of PhOLEDs made with a GNP-based interlayer, formed using GNP solutions having different OD values of 26 (device A), 20 (device B), 13 (device C), and a structurally identical control PhOLED without the GNP-based interlayer (device D). A summary of luminous efficiency and efficiency roll-off measured for different PhOLEDs is given in Table 1. All devices present an efficiency roll-off behavior with increase in the operation current density. However, it is obvious that devices B and C, having a GNP-interlayer between the emitter and the anode, possess enhanced efficiency and a reduced efficiency roll-off behavior as compared to the control device D (without containing GNP-interlayer). Considering the two performance indices of efficiency and efficiency roll-off, PhOLEDs with a GNP-based interlayer, formed using GNP solution having an OD = 13 (device C) is preferred. When the current density increases from 10 to 100 mA/cm^2, a reduction of

Table 1
A summary of luminous efficiency and efficiency roll-off measured for PhOLEDs with a GNP-based interlayer, formed using GNP solutions having different OD values of 26 (device A), 20 (device B), 13 (device C), and a control device without the GNP-based interlayer (device D). The efficiency roll-off is calculated by taking the ratio of the peak luminous efficiency (η_{max}) to the efficiency (η) at the luminance of 50,000 cd/m^2.

Devices	η_{max}	η	Roll-off (%)
A	54.0	50.5	6.4
B	57.3	51.1	10.9
C	69.3	60.0	13.4
D	57.3	44.6	22.2

~10% in the efficiency roll-off is obtained for device C, notably a 70% improvement as compared to the control device D, with an efficiency roll-off of 17%. Inset in Fig. 4 shows the luminance–current efficiency characteristics measured for devices A, B, C and D. The maximum luminous efficiency of 69.3 cd/A at a luminance of 10,507 cd/m^2 is achieved for device C, compared to that of 57.3 cd/A at 5503 cd/m^2 for device D. For PhOLEDs operated at a very high luminance of 50,000 cd/m^2, devices C and D possess an efficiency roll-off of 13.4% and 22.2%, corresponding to a 40% reduction.

Fig. 5 shows the current density–voltage characteristics measured for devices A, B, C, and D. As can be seen, device A has the highest current density under the same operating voltage. These results are in good agreement with the above discussion. It reveals that a larger leakage current is formed in PhOLEDs having an interlayer with higher density of GNPs, caused by the larger-sized GNPs developed during the annealing process as shown in Fig. 1a. It can also be seen in Fig. 4 that the luminous efficiency of the PhOLEDs increases with increase in the density of GNPs on GNP-covered ITO surface, a maximum efficiency is achieved under larger current density for device C. This is due to increased leakage current caused by large sized GNPs in the interlayer. To analyze the effect of GNP surface plasmons on the performance of different PhOLEDs, the EL spectra of devices A, B, C, and D were measured, and the corresponding normalized EL spectra are shown in Fig. 6. It can be seen that devices B and C possess higher emission intensity over the wavelength region from 510 to 550 nm, which overlaps with LSPs excited by GNPs. Compared to devices B and C, a relatively weaker EL emission for device A is observed in the same region. The results reveal the coupling between excitons and GNP LSPs as shown in Fig. 3, implying the GNP density impacts the radiative or non-radiative decay processes of the excitons in the emission layer.

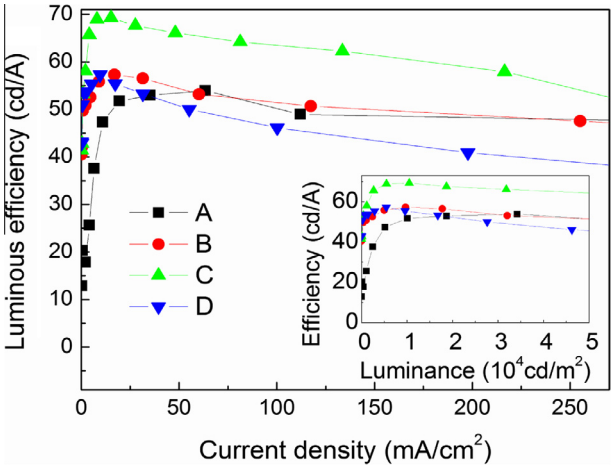

Fig. 4. Luminous efficiency–current density characteristics measured for PhOLEDs with a GNP-based interlayer, formed using GNP solutions having different OD values of 26 (device A), 20 (device B), 13 (device C), and a structurally identical control PhOLED without the GNP-based interlayer (device D). Luminous efficiency–luminance characteristics of devices A, B, C, and D are shown in the inset.

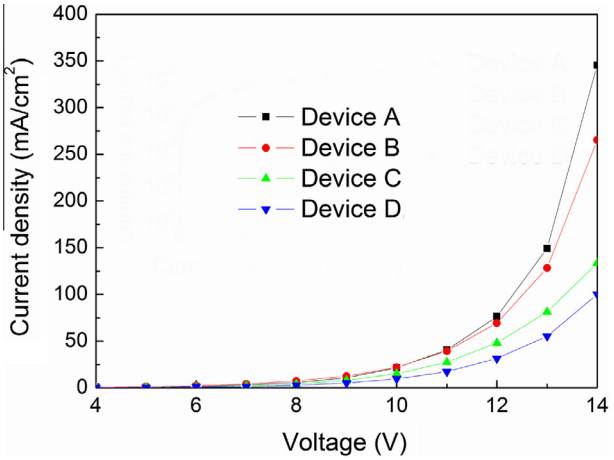

Fig. 5. Current density–voltage characteristics measured for PhOLEDs with a GNP-based interlayer, formed using GNP solutions having different OD values of 26 (device A), 20 (device B), 13 (device C), and a structurally identical control PhOLED without the GNP-based interlayer (device D).

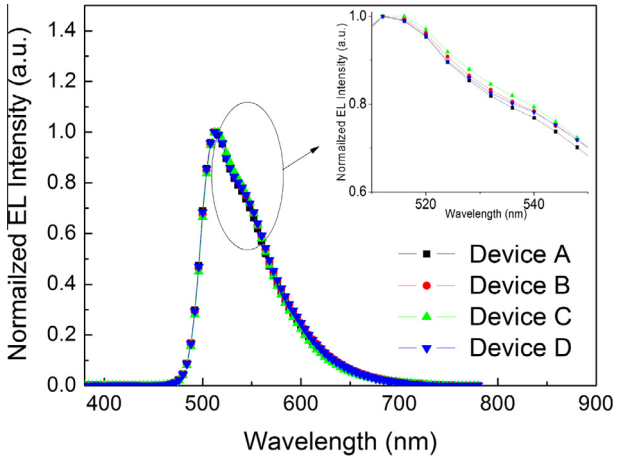

Fig. 6. The normalized EL spectra of devices A, B, C, and D. Inset is the enlarged EL spectra for the wavelength range between 510 and 550 nm.

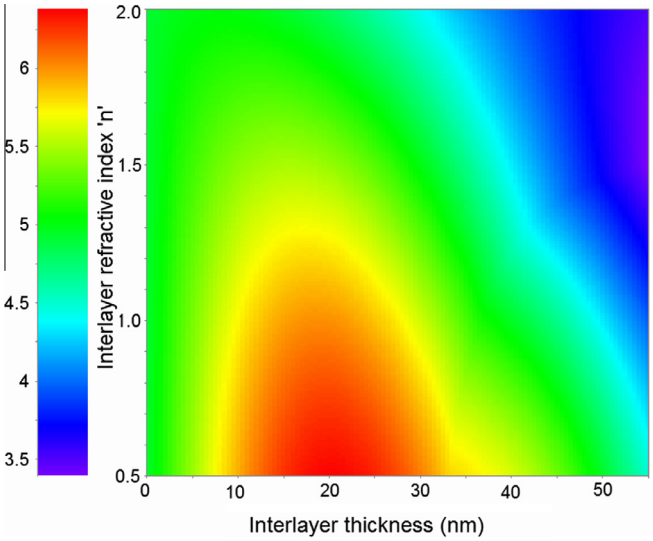

Fig. 7. Contour map of the calculated integrated intensity of EL emission as a function of the effective refractive index and the thickness of the GNP-based interlayer.

PhOLEDs with a configuration of ITO/MoO_3/CBP/CBP:Ir(ppy)$_3$/TPBi/Li/Al do not satisfy a perfect hole–electron current balance, with holes being the majority carriers, resulting in imperfection in the emission efficiency and large efficiency roll-off. This suggests that the use of GNP-modified ITO anode in PhOLEDs, with a configuration of ITO/GNPs/MoO_3/CBP/CBP:Ir(ppy)$_3$/TPBi/Li/Al, is not likely to contribute to the improvement in hole–electron balance. As such, the efficiency difference observed in PhOLEDs made with bare ITO and GNP-modified ITO cannot be simply explained by the difference in electrical characteristics. Therefore, the results thus obtained can be explained due to the coupling between excitons and gold nanoparticle surface plasmons on emission behavior of PhOLEDs, supported by the transient photoluminescence measurements. The experimental results show that PhOLEDs made with GNP-modified ITO allow improving luminous efficiency and reducing efficiency roll-off. Therefore it is anticipated that the performance enhancement in GNP-incorporated PhOLEDs is mainly due to the coupling between excitons and gold nanoparticle surface plasmons.

A low refractive index out-coupling interlayer is often used to improve light out-put in OLEDs [28]. In this work, an enhanced out-coupling efficiency of PhOLEDs having a GNP-interlayer is observed. In order to evaluate the out-coupling effect on improvement in the luminous efficiency, an effective out-coupling layer consisting of a GNP-interlayer, a MoO_3 HIL, and a CBP HTL, sandwiched between the ITO and organic emitter was considered in the simulation. The refractive index of the effective out-coupling layer can be determined by taking into account the volume fraction of each component layer using the dielectric mixing theory [29]. The effect of incorporating GNPs on light out-put of PhOLEDs can then be calculated and compared with the measurements. The intensity of device emission as functions of the refractive index and the thickness of the effective out-coupling layer were calculated using the transfer matrix theory [4,30–32]. An optimization of the structure of the devices was investigated.

The coverage of GNPs (solution-processed) and a 2.0 nm think MoO_3 (thermally evaporated) on ITO surface is of sub-monolayer level. Therefore, the GNP-based interlayer can be regarded as a randomly mixed composite layer consisting of GNPs, MoO_3 and CBP. Using the dielectric mixing theory [29], the average refractive index of the GNP-based interlayer can be estimated based on the different volume ratios of respective components of GNPs, MoO_3 and CBP in the mixture layer. The refractive indices taken for GNP, CBP, ITO, and MoO_3 at wavelength of 532 nm (corresponding the peak emission of Ir(ppy)$_3$) are 0.5, 1.8, 1.9, and 2.0. The effect of the thickness and refractive index of the GNP-based interlayer, varying from 0.5 (the refractive index of GNPs) to 2.0 (the refractive index of MoO_3), on the emission intensity of the devices was analyzed using the transfer matrix theory.

A contour map of the calculated integrated intensity of EL emission as a function of the effective refractive index and the thickness of the mixed out-coupling layer is shown in Fig. 7. It can be seen that maximum emission intensity is obtained when the thickness of the effective out-coupling layer is near 20 nm. For a given thickness of the out-coupling layer, the simulation results reveal that higher emission intensity can be achieved with a low refractive index in the out-coupling layer. The results in Fig. 7 show that over 15% improvement in the emission intensity can be obtained by incorporating a 20 nm thick GNP-based interlayer that holds an effective refractive index of 1.3. The calculation results suggest that the presence of such a GNP-based interlayer also contribute to the efficiency enhancement due to the optical out-coupling effect, thereby the device efficiency as shown in Fig. 4.

4. Conclusion

In summary, enhanced efficiency and reduced efficiency roll-off in Ir(ppy)$_3$-based PhOLEDs were demonstrated by interposing a solution-processed GNP-based interlayer between the anode and the hole-injection layer. The presence of the GNPs in the devices reduces the lifetime of triplet excitons via coupling between excitons and LSPs, suppressing the TTA or/and TPA quenching processes. A coupling mechanism is proposed to illustrate the effect of GNP density on device efficiency roll-off. The GNP-interlayer also acts as an out-coupling layer to enhance light emission, thereby device efficiency. The emission intensity of GNP-incorporated PhOLEDs is dependent on the GNP density in the interlayer and is supported by the theoretical simulation.

Acknowledgments

This work was supported by Natural Science Foundation of China (No. 61205025), Research Grants Council of Hong Kong Special Administrative Region, China, Project No. T23-713/11, and Hong Kong Baptist University Strategic Development Fund (SDF13-0531-A02).

References

[1] B.W. D'Andrade, S.R. Forrest, Adv. Mater. 16 (2004) 1585.
[2] S. Reineke, F. Lindner, G. Schwartz, N. Seidler, K. Walzer, B. Lüssem, K. Leo, Nature 459 (2009) 234.
[3] Y.H. Chen, J.S. Chen, D.G. Ma, D.H. Yan, L.X. Wang, F.R. Zhu, Appl. Phys. Lett. 98 (2011) 243309.
[4] W.H. Choi, H.L. Tam, F.R. Zhu, D.G. Ma, H. Sasabe, J. Kido, Appl. Phys. Lett. 102 (2013) 153308.
[5] C. Adachi, M.A. Baldo, M.E. Thompson, S.R. Forrest, J. Appl. Phys. 90 (2001) 5048.
[6] M.A. Baldo, C. Adachi, S.R. Forrest, Phys. Rev. B 62 (2000) 10967.
[7] S. Reineke, K. Walzer, K. Leo, Phys. Rev. B 75 (2007) 125328.
[8] J.W. Kang, S.H. Lee, H.D. Park, W.I. Jeong, K.M. Yoo, Y.S. Park, J.J. Kim, Appl. Phys. Lett. 90 (2007) 223508.
[9] S.H. Kim, J. Jang, K.S. Yook, J.Y. Lee, Appl. Phys. Lett. 92 (2008) 023513.
[10] T. Zheng, W.C.H. Choy, C.L. Ho, W.Y. Wong, Appl. Phys. Lett. 95 (2009) 133304.
[11] S. Reineke, G. Schwartz, K. Walzer, K. Leo, Appl. Phys. Lett. 91 (2007) 123508.
[12] S. Reineke, G. Schwartz, K. Walzer, M. Falke, K. Leo, Appl. Phys. Lett. 94 (2009) 163305.
[13] F.X. Zang, T.C. Sum, A.C.H. Huan, T.L. Li, W.L. Li, F.R. Zhu, Appl. Phys. Lett. 93 (2008) 023309.
[14] L.M. Zhang, B. Li, L.Y. Zhang, Z.M. Su, ACS Appl. Mat. Interfaces 9 (2009) 1852.
[15] X.Z. Wang, J.W. Ho, Q.Y. Yang, H.L. Tam, G.X. Li, K.W. Cheah, F.R. Zhu, Org. Electron. 12 (2011) 1943.
[16] H. Gao, J. Henzie, T.W. Odom, Nano Lett. 6 (2006) 2104.
[17] Y. Su, Y. Ke, S. Cai, Q. Yao, Light Sci. Appl. 1 (2012) e14.
[18] E. Matioli, S. Brinkley, K. Kelchner, Y. Hu, S. Nakamura, S. DenBaars, J. Speck, C. Weisbuch, Light Sci. Appl. 1 (2012) e22.
[19] C. Xiang, W. Koo, F. So, H. Sasabe, J. Kido, Light Sci. Appl. 2 (2013) e74.
[20] C. Mihalcea, D. Buchel, N. Atoba, J. Tominaga, J. Am. Chem. Soc. 123 (2001) 7172.
[21] A. Choulis, M.K. Mathai, V. Choong, Appl. Phys. Lett. 88 (2006) 213503.
[22] A. Fujiki, T. Uemura, N. Zettsu, M. Akai-Kasaya, A. Saito, Y. Kuwahara, Appl. Phys. Lett. 96 (2010) 043307.
[23] A. Kumar, R. Srivastava, P. Tyagi, D.S. Mehta, M.N. Kamalasanan, Org. Electron. 13 (2012) 159.
[24] W.Y. Ji, L.T. Zhang, W.F. Xie, Opt. Lett. 37 (2012) 2019.
[25] M. Brust, M. Walker, D. Bethell, D.J. Schiffrin, R. Whyman, J. Chem. Soc. Chem. Commun. 7 (1994) 801.
[26] G. Xu, Y. Chen, M. Tazawa, P. Jin, Appl. Phys. Lett. 88 (2006) 043114.
[27] D.R. Jung, J. Kim, S. Nam, C. Nahm, H. Choi, J.I. Kim, J. Lee, C. Kim, B. Park, Appl. Phys. Lett. 99 (2011) 041906.
[28] Y. Sun, S.R. Forrest, Nat. Photon. 2 (2008) 483.
[29] F.R. Zhu, H. Kohara, T. Fuyuki, H. Matsunami, Jpn. J. Appl. Phys. 35 (1996) 3321.
[30] J. Wang, W.Y. Ji, H.B. Zhu, D.D. Zhang, Org. Electron. 14 (2013) 723.
[31] X.Z. Wang, H.L. Tam, K.S. Yong, Z.K. Chen, F.R. Zhu, Org. Electron. 2 (2011) 1429.
[32] D.G. Deppe, C. Lei, C.C. Lin, D.L. Huffaker, J. Mod. Opt. 41 (1994) 325.